GENETICS

Adiponectin receptor 1 variants contribute to hypertrophic cardiomyopathy that can be reversed by rapamycin

Perundurai S. Dhandapany[1,2,3]*†, Soojeong Kang[4]*, Deepak K. Kashyap[1,5], Raksha Rajagopal[6], Nagalingam R. Sundaresan[6], Rajvir Singh[4], Kumarasamy Thangaraj[5,7], Shilpa Jayaprakash[8], Cholenahally N. Manjunath[8], Jayaprakash Shenthar[8], Djamel Lebeche[4,9,10]†

Hypertrophic cardiomyopathy (HCM) is a heterogeneous genetic heart muscle disease characterized by hypertrophy with preserved or increased ejection fraction in the absence of secondary causes. However, recent studies have demonstrated that a substantial proportion of individuals with HCM also have comorbid diabetes mellitus (~10%). Whether genetic variants may contribute a combined phenotype of HCM and diabetes mellitus is not known. Here, using next-generation sequencing methods, we identified novel and ultrarare variants in adiponectin receptor 1 (*ADIPOR1*) as risk factors for HCM. Biochemical studies showed that *ADIPOR1* variants dysregulate glucose and lipid metabolism and cause cardiac hypertrophy through the p38/mammalian target of rapamycin and/or extracellular signal–regulated kinase pathways. A transgenic mouse model expressing an *ADIPOR1* variant displayed cardiomyopathy that recapitulated the cellular findings, and these features were rescued by rapamycin. Our results provide the first evidence that *ADIPOR1* variants can cause HCM and provide new insights into *ADIPOR1* regulation.

INTRODUCTION

Hypertrophic cardiomyopathy (HCM) is a heterogeneous genetic heart muscle disease affecting 1 of every 500 persons (*1*, *2*). Individuals with HCM are at an increased risk of heart failure and sudden cardiac death (*1*). Usually, HCM is characterized by cardiac hypertrophy with preserved or increased ejection fraction (EF) and cardiac contractility in the absence of secondary causes. HCM is predominantly caused by mutations in sarcomeric protein–encoding genes, most frequently in myosin binding protein C3 (*MYBPC3*) or β-myosin heavy chain 7 (*MYH7*) (*1*–*5*). Notably, 30 to 40% of patients with HCM are negative for sarcomeric genes and exhibit HCM with unknown causes (*1*–*4*). Recent emerging evidence suggests that ~10% of HCM cases coexist with diabetes mellitus in the absence of hypertension and obesity (*3*).

Nonsarcomeric proteins, including adiponectin (APN) and its receptors such as ADIPOR1, have also been implicated in left ventricular (LV) hypertrophy, diabetes, and cardiac energy metabolism (*6*–*9*). Studies have shown that APN protects the heart against ischemia-reperfusion injury and inhibits myocardial apoptosis and pressure overload–induced cardiac hypertrophic remodeling through AMP-activated protein (AMPK)–dependent mechanisms (*6*–*9*). APN also inhibited agonist-stimulated cardiac hypertrophy via ADIPOR1, and knockdown of ADIPOR1 in cardiomyocytes suppresses the effects of APN (*10*). Notably, mutations in the human APN gene (*ADIPOQ*) are associated with type 2 diabetes and cardiovascular disease (*11*, *12*). However, to date, human variants in *ADIPOR1* have not been reported as causes of HCM.

Here, we show that gain-of-function variants in *ADIPOR1* are predominantly found in HCM patients with diabetes. Note that no potential disease-causing pathological mutations were observed in any of the known sarcomeric or diabetes-associated genes in ADIPOR1 genotype–positive patients. The functional characterization of the observed *ADIPOR1* variants using cellular and mouse models suggested that the pathogenesis depends on the hyperactivation of the p38/mammalian target of rapamycin (mTOR) and/or extracellular signal–regulated kinase (ERK) pathways, which can be reversed using the mTOR inhibitor (rapamycin).

RESULTS

Analysis and identification of *ADIPOR1* variants

Families of South Asian (Indian) patients with HCM coexisting with diabetes were designated cohort 1. Patients with other hypertrophy-associated conditions, including hypertension, obesity, and infiltrative cardiovascular diseases, were excluded from cohort 1 (table S1A). Next, we performed trio whole exome sequencing of the unrelated patient families from cohort 1 (table S1, A to D, and Materials and Methods). We identified a novel and potential gene variant in the coding sequences of *ADIPOR1* (c.470T to A) in a patient P1 (fig. S1). The patient's healthy family members (P1a to P1e) screened negative for the particular variant. In the individual *ADIPOR1* variant, the leucine residue at the 157th position was altered to a histidine residue (p.L157H) (Fig. 1A and fig. S1). Our trio exome analysis confirmed that the variant is de novo in nature and novel since it is absent

[1]Centre for Cardiovascular Biology and Disease, Institute for Stem Cell Science and Regenerative Medicine (inStem), Bangalore, India. [2]The Knight Cardiovascular Institute, Oregon Health and Science University, Portland, OR 97239, USA. [3]Departments of Medicine, Molecular, and Medical Genetics, Oregon Health and Science University, Portland, OR 97239, USA. [4]Cardiovascular Research Center, Department of Medicine, Icahn School of Medicine at Mount Sinai, One Gustave L. Levy Place, New York, NY 10029, USA. [5]CSIR–Center for Cellular and Molecular Biology, Hyderabad, India. [6]Department of Microbiology and Cell Biology, Indian Institute of Science, CV Raman Avenue, Bangalore, India. [7]Centre for DNA Fingerprinting and Diagnostics (CDFD), Hyderabad, India. [8]Department of Cardiology, Sri Jayadeva Institute of Cardiovascular Sciences and Research, Bengaluru, India. [9]Graduate School of Biological Sciences, Icahn School of Medicine at Mount Sinai, New York, NY 10029, USA. [10]Department of Medicine, Diabetes, Obesity, and Metabolism Institute, Icahn School of Medicine at Mount Sinai, New York, NY 10029, USA.
*These authors contributed equally to this work as co-first authors.
†Corresponding author. Email: dhan@instem.res.in (P.S.D.); djamel.lebeche@mssm.edu (D.L.)

in the available public databases from diverse world populations, including Single-Nucleotide Polymorphism database (dbSNP), 1000 Genomes Project, National Heart Lung and Blood Institute-Grand Opportunity (NHLBI-GO) Exome Sequencing Project (ESP), Korean exomes database (KOVA), Exome Aggregation Consortium (ExAC), Genome Aggregation Consortium (gnomAD), Trans-Omics for Precision Medicine (TOPMed), and Genotype to Mendelian Phenotype ($Geno_2MP$ v2.2) cohorts, which comprise approximately 426,060 alleles. Notably, the variant is also absent in the recently released Genome Asia 100K consortium dataset, which includes 1196 Indian-specific alleles (fig. S1 and table S1E).

Next, we performed targeted resequencing of *ADIPOR1* in two independent cohorts (table S1A, cohorts 2 and 3) comprising 485 primary HCM patients with and without diabetes. We identified an additional gene variant (c.436G to A), which results in the valine residue at the 146th position being changed to a methionine residue (p.V146M), in three HCM patients with overt diabetes (P2, P3, and P4) belonging to two different families (Fig. 1A, families 2 and 3, table S1D, and fig. S2A). We also observed this ultrarare pathogenic amino acid change in various global populations, including patients with cardiac and metabolic syndrome–associated disorders (table S1E). In cohort 2, we observed another novel variant in the coding sequences of *ADIPOR1* (c.433T to A), which results in an amino acid change from phenylalanine to isoleucine at the 145th position (p.F145I), in an HCM patient without diabetes (Fig. 1A, family 4, P5). This variant is unique and absent in all the above public databases. In addition, all the observed variants were absent in 675 secondary HCM patients with and without diabetes (cohort 3; table S1A), 548 patients with dilated cardiomyopathy with and without diabetes (cohort 4; table S1A), 800 patients with diabetes alone (cohort 5; table S1A), healthy South Indians over the age of 80 (www.idhans.org) (cohort 6; table S1E), and a regional control group comprising 1800 Indian individuals without metabolic or cardiovascular diseases and whose ancestry was confirmed by principal components analysis using specific ancestry markers (cohort 7; table S1E) (*5*).

The amino acids at the 145th, 146th, and 157th positions in *ADIPOR1* are evolutionarily conserved among vertebrate orthologs (Fig. 1B), and the amino acid changes in the respective patients are predicted to be pathological by various in silico software (Fig. 1C). Patients P1, P2, and P4 with HCM showed features of diabetes. However, patient P3 with HCM, who harbors V146M, did not show any metabolic syndrome. However, the risk for developing metabolic syndrome in this particular patient cannot be excluded given the young age of the patient (19 years old), the nature of the pathological variant (functional aspects described below), and the family history of the patient. The HCM patient with the F145I variant (P5) is a relatively older individual (65 years old) with no signs of metabolic syndrome to date. The elder brother and parents of the F145I carrier are healthy and negative for this particular variant. The healthy parents of three of the genotype-positive patient families (Fig. 1A, families 1, 3, and 4) with confirmed paternity are negative for these *ADIPOR1* variants, suggesting a de novo origin and further supporting the role of these variants in cardiomyopathy.

ADIPOR1 variants induce cardiomyocyte hypertrophy

To elucidate the functional consequences of *ADIPOR1* variants, we expressed the representative variants in neonatal rat cardiomyocytes (NRCMs) by transfection with adenoviral vectors (Ad.V146M or

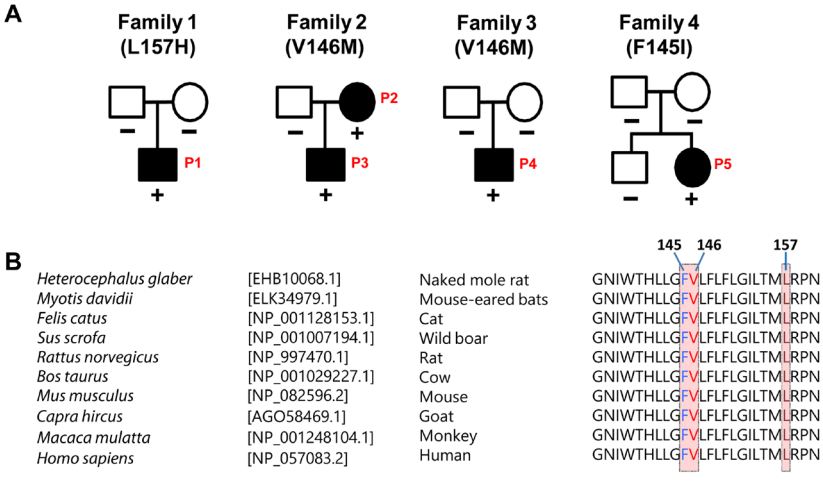

C

Exon	Nucleotide change	Amino acid change	SIFT	Polyphen2	PANTHER-PSEP	MetaDome	Mutation Taster	PMUT	CADD
4	c.470T>A	L157H	Affect protein function (0.01)	Possibly damaging (0.85)	Probably damaging	Intolerant (0.30)	Disease causing (99)	Disease (0.68)	Disease (25.5)
4	c.436G>A	V146M	Affect protein function (0.01)	Possibly damaging (0.9)	Probably damaging	Intolerant (0.33)	Disease causing (21)	Neutral (0.38)	Disease (22.2)
4	c.433T>A	F145I	Affect protein function (0.01)	Possibly damaging (0.63)	Probably damaging	Intolerant (0.36)	Disease causing (21)	Disease (0.53)	Disease (25.2)

Fig. 1. *ADIPOR1* variants in patients with HCM. (**A**) Pedigrees of HCM families with respective *ADIPOR1* amino acid changes. Filled symbols represent affected individuals. Plus (+) and minus (–) signs indicate the presence and absence of the amino acid changes, respectively. (**B**) Alignment of *ADIPOR1* protein sequences from various species with the amino acid changes altered in patients with HCM shown in highlights. (**C**) In silico analysis of the *ADIPOR1* amino acid changes showing the predicted pathological nature. SIFT, Sorting Intolerant From Tolerant; PANTHER-PSEP, protein analysis through evolutionary relationships position-specific evolutionary preservation; PMUT, pathogenic mutation prediction; CADD, combined annotation dependent depletion.

Ad.F145I) or transfected NRCMs with a control (Ad.βGal) or wild-type (Ad.AR1) vector and assessed hypertrophic markers, including cell surface area and fetal gene expression. The transient expression of the mutant proteins in NRCMs resulted in significant increases in cell size (Fig. 2, A and B) and the expression of fetal genes expression, including atrial natriuretic factor (*Anf*), brain natriuretic peptide (*Bnp*) (except in Ad.F145I-expressing NRCMs), and β-myosin heavy chain (*Myh7*), compared with those observed in NRCMs transfected with Ad.βGal or Ad.AR1 (Fig. 2C). A similar pattern was also observed for Ad.L157H-expressing cardiomyocytes (fig. S2, B and C). These data suggest that the constitutive expression of *ADIPOR1* mutants can induce the cardiac hypertrophic response.

ADIPOR1 variants stimulate hypertrophy via p38/mTOR- and/or ERK-dependent mechanisms

Next, we examined the signaling pathways modulated by *ADIPOR1* variants by assessing the effects of the variants on lysates obtained from cardiomyocytes expressing Ad.AR1, Ad.F145I, Ad.V146M, or Ad.L157H using immunoblotting for various downstream targets. Unexpectedly, the levels of well-known downstream targets of *ADIPOR1*, including AMPK, liver kinase B1 (LKB1), and acetyl–coenzyme A (CoA) carboxylase (ACC), were relatively normal in the cardiomyocytes expressing Ad.V146M compared to those expressing Ad.AR1 (Fig. 3A). Next, we explored an alternative downstream pathway known to be associated with *ADIPOR1* signaling involving p38 kinase and mTOR. Compared to Ad.AR1-expressing cardiomyocytes, Ad.V146M-expressing cardiomyocytes showed increased phosphorylation of p38/mTOR, 70-kDa ribosomal protein S6 kinase ($p70^{S6K}$), and eukaryotic elongation factor–2 kinase (eEF2K) and decreased activity of eEF2, a downstream target of the mTOR pathway (Fig. 3, A and B). However, compared to Ad.AR1-expressing cardiomyocytes, they showed normal levels of ERK1/2 and cytochrome oxidase subunit 2 (COX2) (Fig. 3A). A similar pattern was observed in cardiomyocytes expressing Ad.L157H compared to those expressing Ad.AR1 (fig. S2, D and E). Furthermore, stimulation with a known agonist (APN) failed to inhibit the AR1V146M-induced activation of p38/mTOR (fig. S3), suggesting that the known protective effects of APN are lost in AR1V146M-expressing cells. Treatment with known inhibitors of p38 and mTOR rescued cardiomyocyte hypertrophy and restored normal signaling in cells expressing a representative mutant (Ad.V146M), respectively (fig. S4, A to F, respectively). In contrast, Ad.F145I activated cellular hypertrophy through ERK1/2 but not the p38/mTOR pathway (Fig. 3, C and D), and this cellular hypertrophy was rescued by a well-established ERK1/2 inhibitor (fig. S5). These data indicate that Ad.V146M and Ad.L157H acted through different signaling pathways than Ad.F145I to induce cardiac hypertrophy. These findings demonstrate that the position and the type of amino acid change in *ADIPOR1* are crucial for the downstream signaling of *ADIPOR1* and disease pathogenesis. This might partly explain the differences in patient phenotypes; the V146M and L157H variants are associated with HCM with diabetes, while the F145I variant is associated with HCM alone.

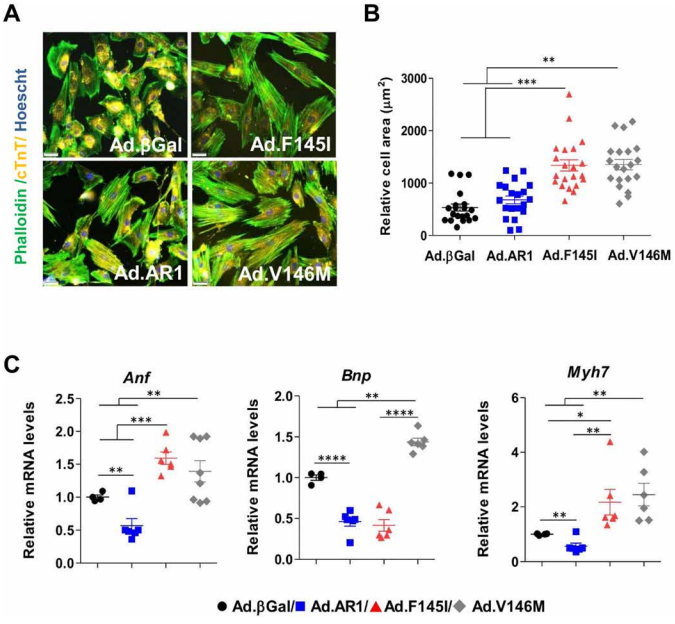

Fig. 2. *ADIPOR1* variants induce cardiomyocyte hypertrophy. Representative images (**A**) and cell surface area measurements (**B**) in cardiomyocytes infected with Ad.βGal (vector control), Ad.AR1, Ad.F145I, and Ad.V146M and stained with phalloidin (actin), cardiac troponin T (cTnT), or Hoechst (nuclei) as indicated. Scale bars, 10 μm. Results presented as relative cell area compared to Ad.βGal ($n = 20$ cells in five different fields). (**C**) Quantitative reverse transcription polymerase chain reaction (RT-PCR) analysis of hypertrophic marker genes *Anf*, *Bnp*, and *Myh7* in cardiomyocytes infected with Ad.βGal, Ad.AR1, Ad.F145I, and Ad.V146M, respectively. mRNA levels were normalized to 18*S* ribosomal RNA (rRNA) and presented as relative expression levels compared to the level in the Ad.βGal cardiomyocytes ($n = 4$ to 8). Values are shown as means ± SEM with each experiment performed in triplicate ($n = 3$). Significance was evaluated by Student's *t* test or one-way analysis of variance (ANOVA) with post hoc Bonferroni's test, respectively. *$P < 0.05$, **$P < 0.01$, ***$P < 0.001$, and ****$P < 0.0001$.

The *ADIPOR1* V146M variant interferes with glucose transport and insulin responsiveness

ADIPOR1 is a key regulator of glucose and fatty acid metabolism (*13*–*15*). To test whether *ADIPOR1* variants affect these processes, we measured glucose uptake and glucose metabolism-related genes in adult rat cardiomyocytes expressing Ad.V146M (a relatively common variant that we observed in HCM patients with diabetes) along with Ad.AR1. Glucose uptake was reduced (Fig. 4A), and the expression of genes that regulate glucose utilization, such as solute carrier family 2 member 4 (*Slc2a4*) and phosphofructokinase and muscle-type gene (*Pfkm*; regulates glycolysis in the cytosol), was differentially modulated in cardiomyocytes expressing Ad.V146M compared to those expressing Ad.AR1 (Fig. 4B). Simultaneously, cardiomyocytes expressing Ad.V146M showed increased serine phosphorylation of insulin receptor substrate–1 (IRS1) (Fig. 4C). In addition, decreased phosphorylation of IRS1 tyrosine, AKT, and PFK2 (phosphofructokinase-2) was observed compared to cardiomyocytes expressing Ad.AR1 (Fig. 4D). All these signaling alterations suggest decreased insulin sensitivity. In contrast, treatment with rapamycin attenuated IRS1 serine phosphorylation and restored the expression of *Slc2a4* and *Pfkm* (Fig. 4, C, E, and F).

ADIPOR1 V146M facilitates lipid uptake and oxidation

Next, we measured the palmitate uptake rates and the relative expression levels of genes involved in lipid oxidation in cardiomyocytes expressing Ad.βGal, Ad.AR1, or Ad.V146M. Palmitate uptake was increased in agonist-treated or untreated Ad.V146M-expressing cardiomyocytes compared to Ad.AR1-expressing cardiomyocytes (fig. S6A). The expression of genes involved in lipid oxidation,

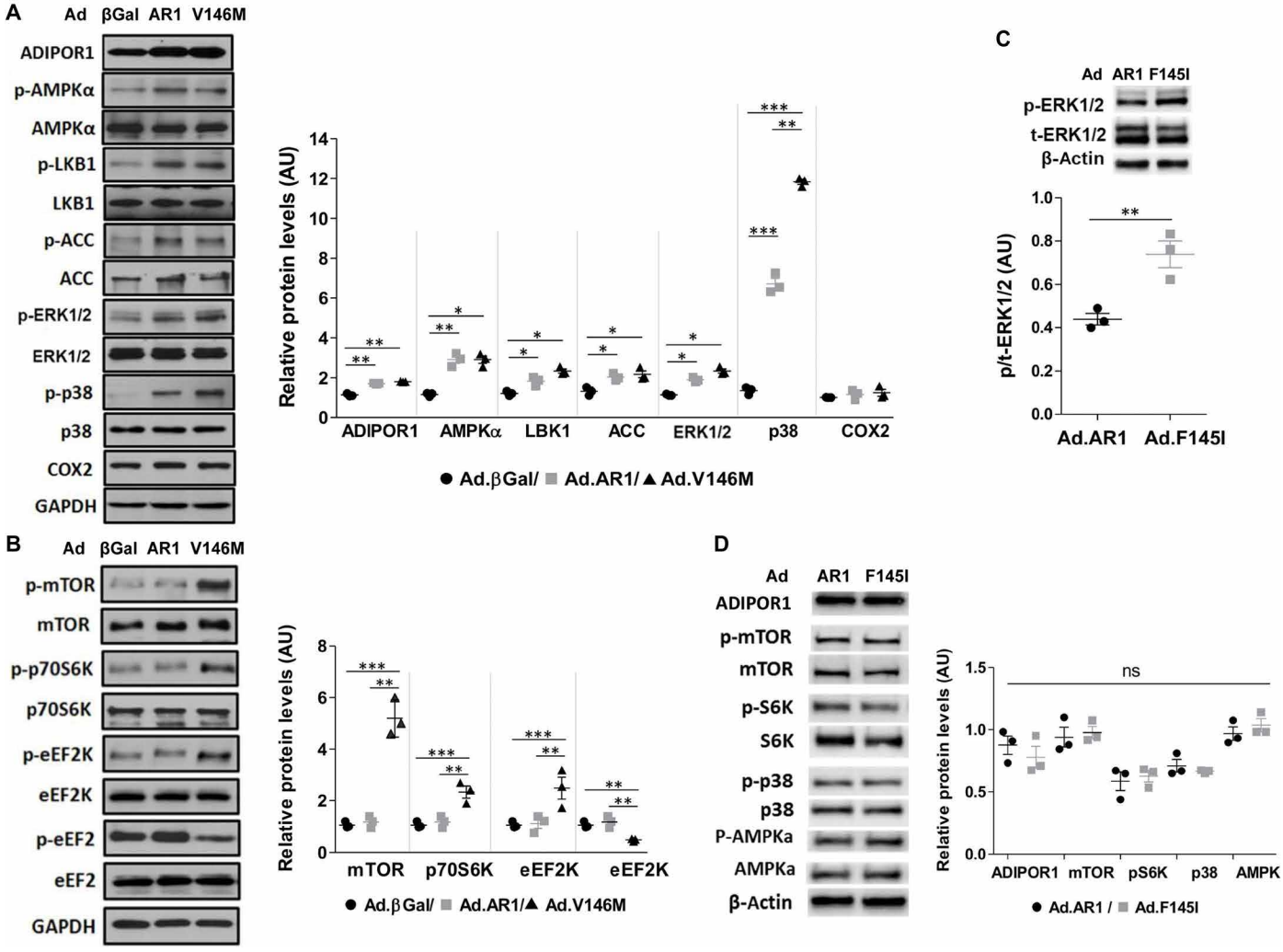

Fig. 3. Individual *ADIPOR1* variants modulate diverse signaling pathways in cardiomyocyte hypertrophy. (**A** to **D**) Representative immunoblots with respective proteins from the total lysates of neonatal cardiomyocytes expressing Ad.βGal, Ad.AR1, Ad.V146M (A and B), or Ad.F145I (C and D), respectively. Expression levels were normalized to respective total proteins and presented as relative expression levels compared to the level in the Ad.βGal or Ad.AR1 cardiomyocytes, respectively. Glyceraldehyde-3-phosphate dehydrogenase (GAPDH) or β-actin levels were used as a loading control. Values are shown as means ± SEM with each experiment performed in triplicate ($n = 3$). Significance was evaluated by Student's *t* test or one-way ANOVA with post hoc Bonferroni's test, respectively. *$P < 0.05$, **$P < 0.01$, and ***$P < 0.001$. AU, arbitrary units.

including fatty acid transporter (*Slc27a1*), acyl-CoA oxidase (*Acox1*; peroxisomal β-oxidation), carnitine palmitoyltransferase 1 (*Cpt1a*; involved in mitochondrial fatty acid uptake), peroxisome proliferator–activated receptor γ coactivator 1α (*Ppargc1a*), and peroxisome proliferator–activated receptor α (*Ppara*), was noticeably up-regulated in Ad.V146M-expressing cardiomyocytes compared to Ad.βGal- or Ad.AR1-expressing cardiomyocytes (fig. S6B). Notably, the activation of PPARα is known to control key transcription genes involved in the metabolism of fatty acid β-oxidation (*16*). Pharmacological inhibition of the p38 pathway significantly reduced the expression of *Ppara* and *Cpt1a* in cardiomyocytes expressing Ad.V146M mutant compared to those expressing Ad.AR1 (fig. S6, C and D). Collectively, these data suggest that Ad.V146M mediates insulin resistance and lipid utilization through the regulation of the p38/mTOR pathways.

Transgenic mice with an *ADIPOR1* variant exhibit cardiac hypertrophy, fibrosis, and metabolic defects

To test whether *ADIPOR1* variants can independently induce cardiomyopathy, we generated transgenic mice that specifically expressed a representative green fluorescent–tagged human variant proteins (Cre-V146M) in the heart (fig. S7, A and B). At the age of 8 to 12 weeks, the Cre-V146M transgenic mice displayed increase in the heart-to-body weight ratio (fig. S7C), the myocyte cross-sectional area (fig. S7D), the expression of fetal genes (*Anf*, *Bnp*, and *Myh7*) (fig. S7E), and myocardial fibrosis (fig. S7F) compared to those in the controls (Cre mice) after tamoxifen treatment, respectively. Notably, p38 and mTOR (but not ERK1/2) activation and the associated metabolic alterations elicited by Ad.V146M in the cellular models were also altered in Cre-V146M mice compared to Cre mice (Fig. 5A). The expression of lipid oxidation genes, including *Slc27a1*,

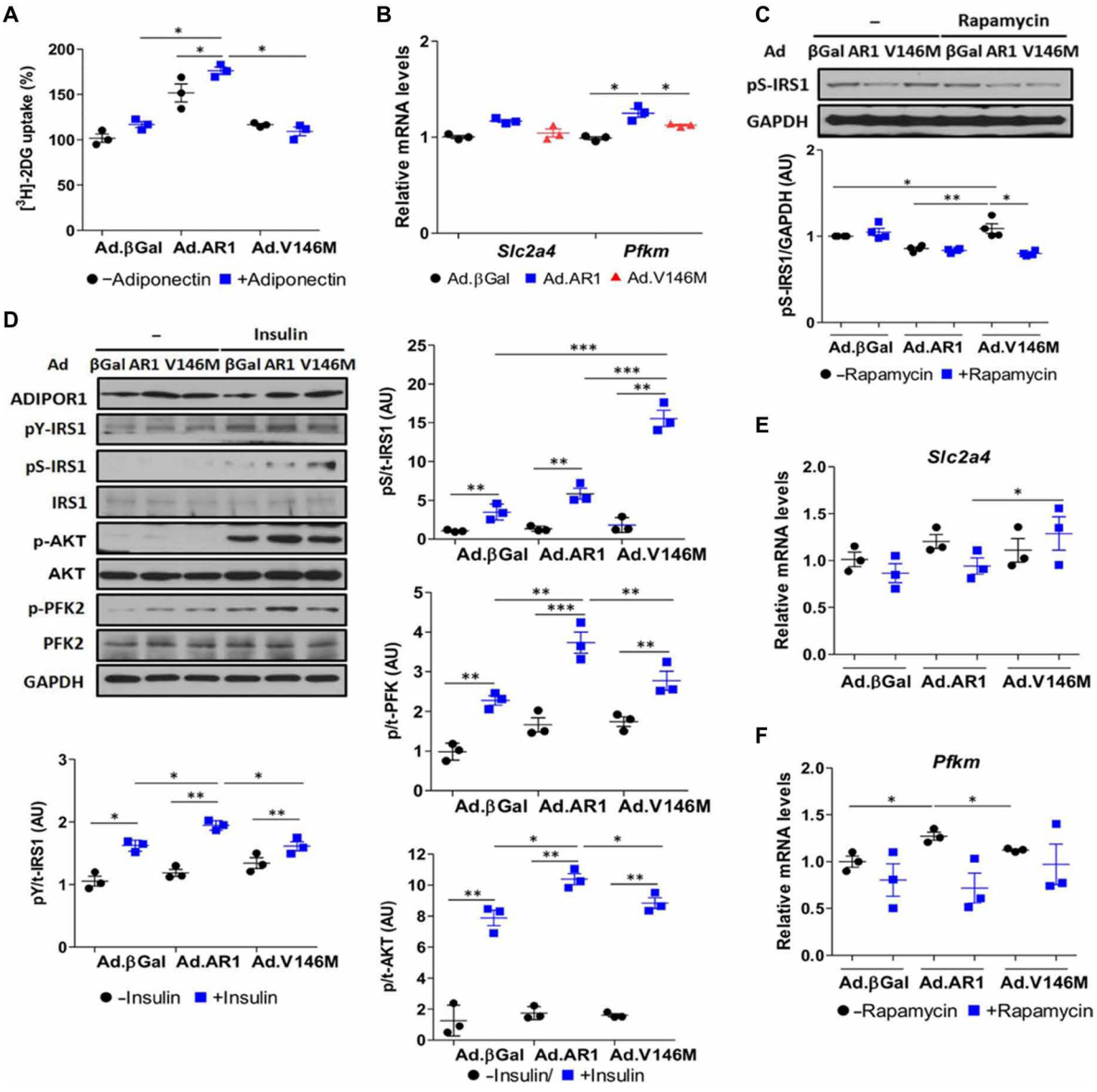

Fig. 4. *ADIPOR1* V146M interferes with glucose transport and insulin response in cardiomyocytes. (**A**) Measurement of glucose uptake rates in adult rat cardiomyocytes expressing Ad.βGal, Ad.AR1, and Ad.V146M [APN treatment (±30 μg/ml) for 30 min]. The uptake rates were determined using [^{3}H]–2-deoxyglucose (2DG) incorporation method with counts expressed in counts per minute and plotted as a percentage to the Ad.βGal. Data are displayed as the percentage difference in uptake relative to basal values ($n = 3$). (**B**) Quantitative RT-PCR analysis of glucose utilization–related genes (*Slc2a4* and *Pfkm*) in adult cardiomyocytes expressing Ad.βGal, Ad.AR1, and Ad.V146M. mRNA levels were normalized to 18*S* rRNA and presented as relative expression levels compared to the level in the Ad.βGal cardiomyocytes ($n = 4$ to 8). (**C** and **D**) Representative immunoblots with respective proteins from the total lysates of adult cardiomyocytes expressing Ad.βGal, Ad.AR1, and Ad.V146M (±100 nM rapamycin treatment for 30 min or ±100 nM insulin treatment for 15 min), respectively. Expression levels of phospho-proteins were normalized to respective total proteins and presented as relative expression levels and compared accordingly. GAPDH levels were used as loading control. (**E** and **F**) Quantitative RT-PCR analysis of glucose utilization–related genes (*Slc2a4* and *Pfkm*) in adult rat cardiomyocytes expressing Ad.βGal, Ad.AR1, and Ad.V146M (±100 nM rapamycin treatment for 30 min). mRNA levels were normalized to 18*S* rRNA and presented as relative expression levels compared to the level in the untreated Ad.βGal cardiomyocytes ($n = 3$). All the values are shown as means ± SEM with each experiment performed in duplicate. Significance was evaluated by Student's *t* test or one-way ANOVA with post hoc Bonferroni's test, respectively. $^*P < 0.05$, $^{**}P < 0.01$, and $^{***}P < 0.001$.

*Acox*1, *Cpt1a*, *Ppargc1a*, and *Ppara*, was up-regulated in Cre-V146M mice compared to Cre mice (Fig. 5B). In addition, the expression of glucose metabolism–related genes, such as *Slc2a1*, *Slc2a4*, and *Pfkm*, was impaired in Cre-V146M mice compared to Cre mice (Fig. 5, C to E). In addition, endomyocardial biopsy from a patient with V146M mutation showed enhanced mTOR activity (Fig. 5F).

Rapamycin rescues cardiac dysfunction in the ADIPOR1 V146M mouse model

To determine whether cardiac changes provoked by the V146M variant of *ADIPOR1* are able to be reversed by silencing mTOR, we treated *ADIPOR1* transgenic mice with rapamycin. Rapamycin has been shown to ameliorate myocyte hypertrophy and attenuate

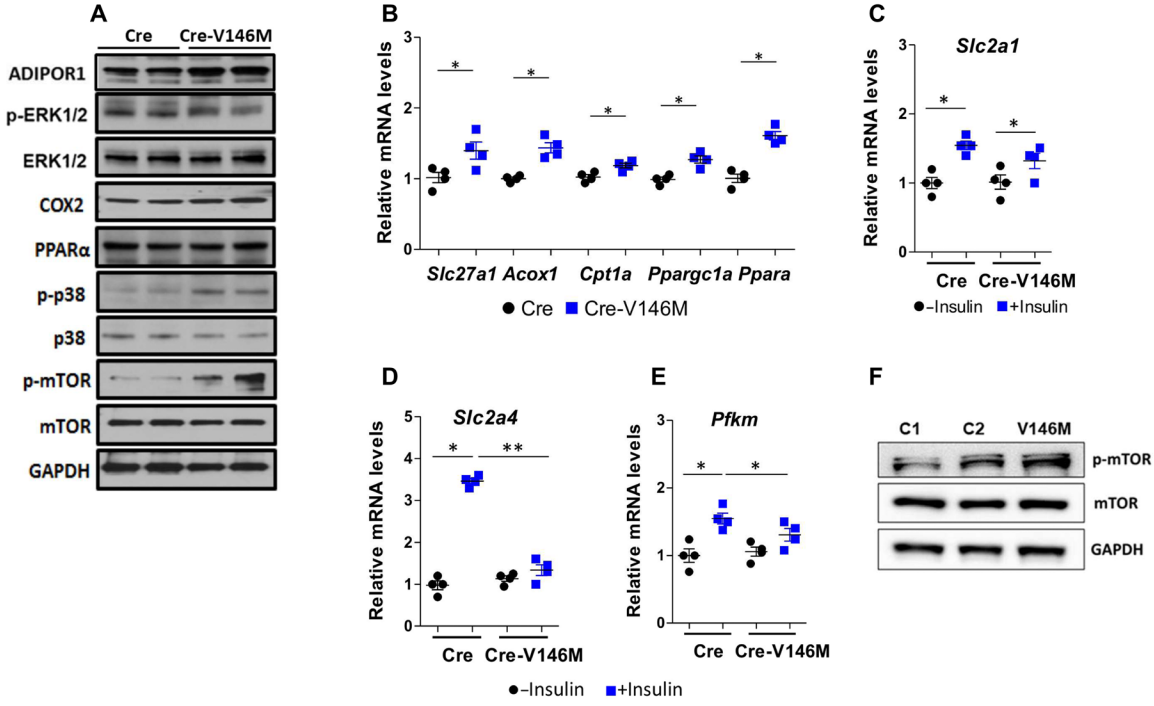

Fig. 5. *ADIPOR1* mutant (Cre-V146M) mice activate p38/mTOR pathways and modulate metabolism-associated gene expressions. (**A**) Representative immunoblots with respective proteins from the total lysates of mouse ventricular tissues isolated from Cre or Cre-V146M ($n = 2$). GAPDH levels were used as loading control. (**B**) Quantitative RT-PCR analyses of lipid oxidation genes (*Slc27a1*, *Acox1*, *Cpt1a*, *Ppargc1a*, and *Ppara*) in Cre or Cre-V146M mice ($n = 4$). (**C** to **E**) Quantitative RT-PCR analyses of glucose utilization genes (*Slc2a1*, *Slc2a4*, and *Pfkm*) in ventricular cardiac tissues from Cre or Cre-V146M groups ($n = 4$) as indicated. Mice were fasted overnight and received a single intraperitoneal injection of insulin (10 mU/g), and hearts were harvested 10 min later. mRNA levels were normalized to 18*S* rRNA and presented as relative expression levels compared to the level in the Cre mouse heart tissues, respectively. Values are shown as means ± SEM with each experiment performed in duplicate. Significance was evaluated by Student's *t* test. $^{*}P < 0.05$ and $^{**}P < 0.01$. (**F**) Representative immunoblots with respective proteins in human heart tissue biopsies from healthy individuals (C1 and C2) or *ADIPOR1* V146M–mutated patient. GAPDH levels were used as loading control.

cardiac remodeling and dysfunction in response to mechanical stress or cardiac injury (*17*–*19*). Rapamycin treatment effectively reversed Cre-V146M–induced cardiac functional deterioration. LV function and dimensions were measured by serial echocardiography at baseline and following vehicle or rapamycin treatment for 30 days; rapamycin (2 mg/kg), a dose equivalent to that used in humans based on body surface area, was administered orally each day (*20*). Cardiac contractility, as assessed by fractional shortening (FS) (Cre-V146M-Veh versus Cre-V146M-Rapa: FS%, 39.68 ± 8.29 versus 63.46 ± 2.23; $P < 0.0001$) (Fig. 6, A and B, and table S1F) and the ejection fraction (EF) (Cre-V146M-Veh versus Cre-V146M-Rapa: EF%, 77.09 ± 8.45 versus 93.68 ± 2.88; $P < 0.01$) (table S1F), and LV internal chamber dimensions were substantially improved in the rapamycin-treated Cre-V146M group compared to vehicle-treated animals (Cre-V146M-Veh versus Cre-V146M-Rapa: LV internal diameter end diastole, 3.50 ± 0.4 mm versus 2.75 ± 0.21 mm; $P < 0.01$; and LV internal diameter end systole: 2.056 ± 0.51 mm versus 1.037 ± 0.13 mm; $P < 0.0001$) (table S1F). Postmortem analysis revealed that the heart weight-to-tibia length ratio was lower in the rapamycin Cre-V146M group (fig. S8, A and B) and paralleled the decrease in echocardiography-derived LV mass (table S1F). We confirmed these observations at the cellular level by evaluating the cross-sectional area of cardiac myocytes in histological sections of LV tissues. We observed that cardiac myocytes from the hearts of vehicle-treated Cre-V146M mice were significantly larger than those from hearts of control mice (Fig. 6C and fig. S8C). In contrast, rapamycin treatment considerably reduced the size of cardiomyocytes so that they were similar in size to those of the controls, indicating an attenuation of cardiac hypertrophy (Fig. 6C and fig. S8C). This reversal in LV remodeling was matched by improvement in cardiac performance accompanied by an enhancement of the sarcoplasmic/endoplasmic reticulum Ca^{2+} ATPase 2 (SERCA2a)/phospholamban (PLN) ratio (Fig. 6D), which led to increased sarcoplasmic reticulum Ca^{2+} cycling and improved contractility. In addition, a reversal in the reinduction of the maladaptive fetal cardiac gene program was characterized by a significant decrease in the mRNA expression of *Anf* and *Myh7* in the Cre-V146M mouse heart after rapamycin treatment was compared to vehicle treatment (Fig. 6E). Since hypertrophy and fibrosis are interrelated events and myocardial fibrosis is a prominent feature of HCM, we sought to examine the potential impact of mTOR inhibition on the regulation of cardiac extracellular matrix remodeling. Histological examination of LV sections by Masson's trichrome staining and subsequent quantification of the fibrotic area revealed that vehicle-treated Cre-V146M mice exhibited a profound increase in interstitial fibrosis in the heart compared with that in control hearts (Fig. 7A). In contrast, rapamycin treatment significantly decreased fibrosis both interstitially (Fig. 7A) and perivascularly (fig. S8D). Note that rapamycin itself failed to alter FS%, EF%, cardiomyocyte cross-sectional area, or fibrogenesis in control mouse hearts (Figs. 6, A to E, and 7A and table S1F). Blockade of mTOR by rapamycin was confirmed by the attenuation of mTOR phosphorylation and $p70^{S6K}$ protein activation (Fig. 7, B and C). Thus, our findings provide evidence that *ADIPOR1* variant causes cardiomyopathy that can be rescued by rapamycin.

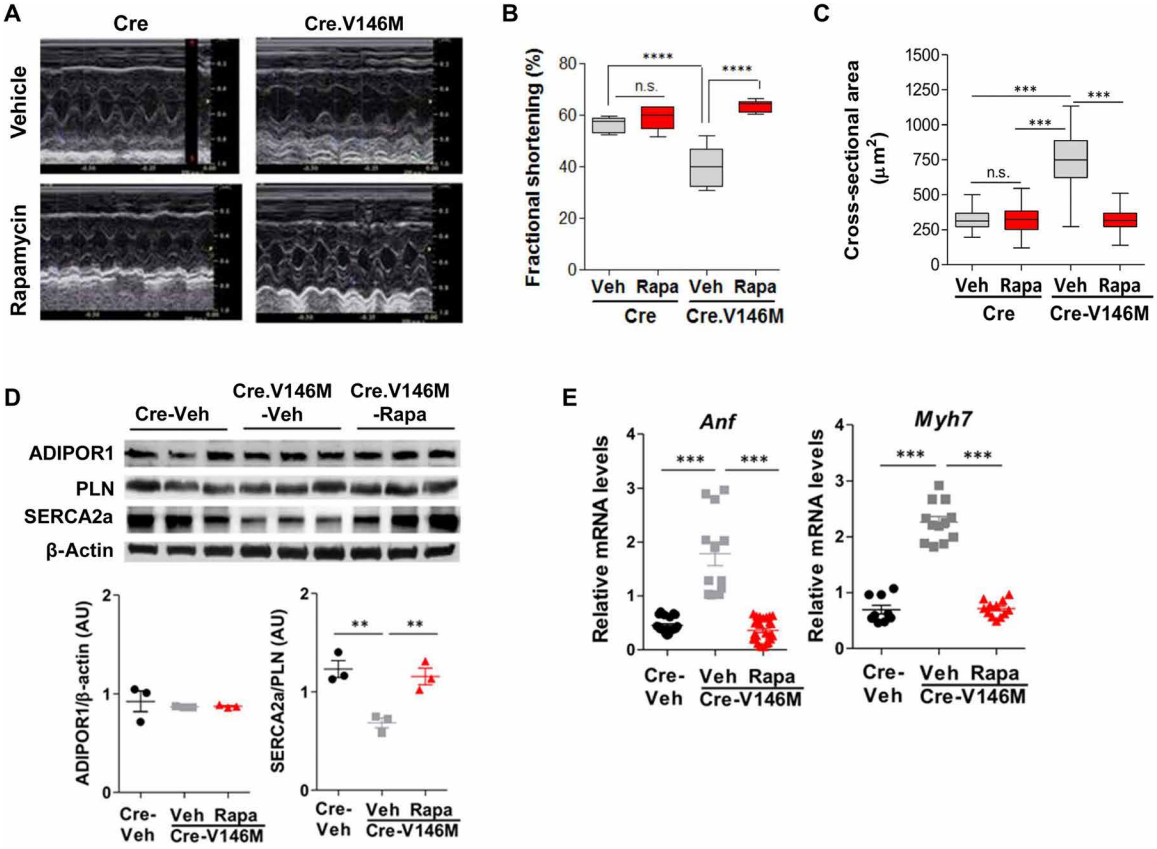

Fig. 6. Rapamycin reverses cardiac failure in ADIPOR1 Cre-V146M mice. (**A**) Representative M-mode echocardiography and (**B**) percentage FS in vehicle or rapamycin-treated Cre and Cre-V146M mice (Cre-Veh, Cre.V146M-Veh, or Cre.V146M-Rapa), respectively ($n = 12$). n.s., not significant. (**C**) Representative immunoblots with indicated proteins from the total lysates of the respective mouse heart tissues (Cre-Veh, Cre.V146M-Veh, or Cre.V146M-Rapa) ($n = 3$). Expression levels were normalized to respective total proteins and presented as relative expression levels compared to the level in Cre-Veh or Cre.V146M-Veh. β-Actin levels were used as loading control. (**D**) Representative cardiomyocyte cross-sectional area (in square micrometers) measurements ($n = 5$ and 20 to 30 cells per mouse) in Cre-Veh, Cre-Rapa, Cre.V146M-Veh, and Cre.V146M-Rapa mouse ventricular sections, respectively. (**E**) Quantitative RT-PCR analysis of hypertrophic-related genes (*Anf* and *Myh7*) in heart tissues from Cre-Veh, Cre.V146M-Veh, and Cre.V146M-Rapa. mRNA levels were normalized to 18*S* rRNA and presented as relative expression levels compared to the levels in the Cre-Veh or Cre.V146M-Veh. Individual experiment was performed in duplicate ($n = 9$ to 12), respectively. All the values are shown as means ± SEM. Significance was evaluated by Student's *t* test or one-way ANOVA with post hoc Bonferroni's test, respectively. $^{**}P < 0.01$, $^{***}P < 0.001$, and $^{****}P < 0.0001$.

DISCUSSION

Our genetic screening and subsequent validation using a total of 2552 cardiomyopathy patients with and without metabolic disorders along with 1894 respective healthy controls resulted in the identification of previously unknown and ultrarare variants of the *ADIPOR1* gene. In the gene discovery phase, we used a stringent criterion by selecting HCM patients with diabetes alone for our exome analysis. Notably, the selected patients were negative for known pathogenic mutations in different sarcomeric and diabetes-related genes known to be associated with HCM and metabolic disorders, which together account for ~70% of known HCM cases. These data suggest that the identified variants might determine patient phenotypes. This approach led to the unbiased discovery of *ADIPOR1* as a candidate gene. We also replicated the *ADIPOR1* variants in HCM of unrelated patient cohorts. Computational analyses predicted that the identified *ADIPOR1* mutations cause significant damage to and potential pathological effects on protein structure and function. Overall, the frequency of total missense variants of the *ADIPOR1* gene was significantly higher among patients with diabetic-associated cardiomyopathy in our cohort than in the different populations comprising 215,522 unrelated individuals (5/1058 versus 201/431,044; $P \leq 0.0001$; table S1E). Thus, *ADIPOR1* variants are strongly associated with cardiomyopathy (patients with primary HCM versus global unmatched populations: odds ratio, 9.7; 95% confidence interval, 4 to 23; table S1E). Evaluations of the functional relevance of the identified variants in cellular and transgenic animal models revealed that ADIPOR1 mutations are associated with hypertrophic remodeling and cardiometabolic abnormalities. These findings outline a strong and shared genetic link between metabolic syndrome and HCM.

ADIPOR1 mutants recapitulate human cardiomyopathy

APN and its receptors have been widely reported to elicit their pleiotropic and antihypertrophic responses through the activation of AMPK (*6*, *7*, *9*, *14*). Overexpression of wild-type *ADIPOR1* attenuates lipid accumulation and cardiac hypertrophy associated with high-fat/sucrose diet–induced obesity in mice (*21*). Mutations in *PRKAG2* (an AMPK subunit) lead to glycogen storage cardiomyopathy. In the hearts of transgenic PRKAG2 mice, the myocytes are distended and exhibit vacuolated cytoplasm without fibrosis due to AMPK dysregulation (*22*–*24*). In contrast, our study demonstrates

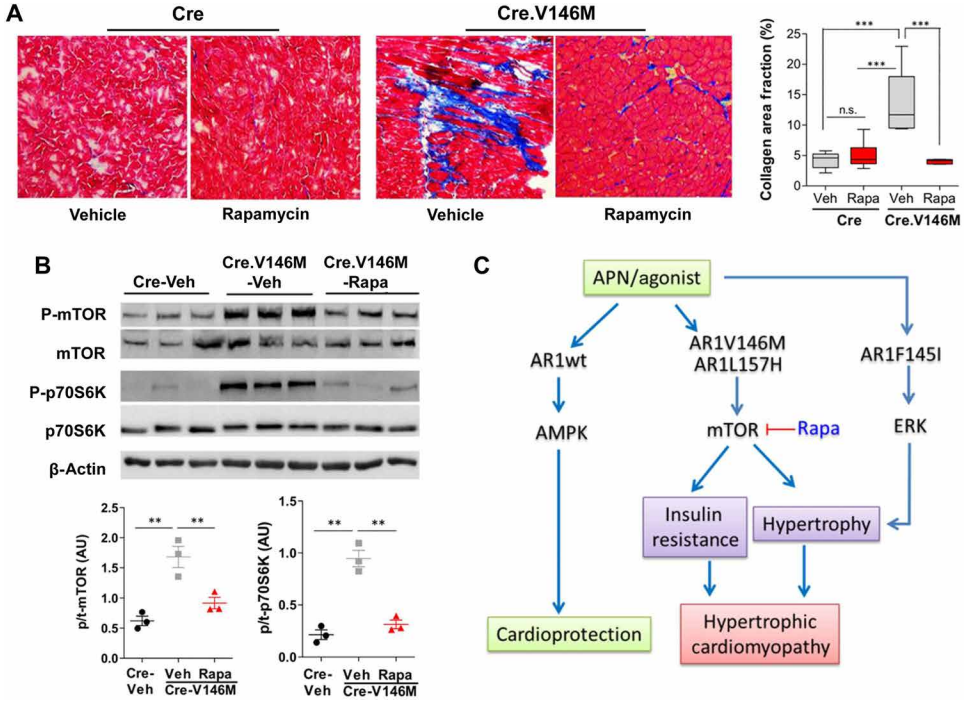

Fig. 7. Rapamycin reduces cardiac fibrosis and restores mTOR pathway in ADIPOR1 Cre-V146M mice. (**A**) Representative micrographs of Masson's trichrome–stained LV sections and quantification of fibrosis (collagen area) in the indicated mice, respectively ($n = 5$, four to five fields per mouse). (**B**) Representative immunoblots with respective proteins from the total lysates of mouse ventricular tissues isolated from Cre-Veh, Cre.V146M-Veh, or Cre.V146M-Rapa ($n = 3$). Expression levels were normalized to respective total proteins and presented as relative expression levels compared to the level in Cre-Veh or Cre.V146M-Veh, respectively. β-Actin levels were used as loading control. All the values are shown as means ± SEM. Significance was evaluated by Student's *t* test or one-way ANOVA with post hoc Bonferroni's test, respectively. $^{**}P < 0.01$ and $^{***}P < 0.001$. (**C**) Proposed mechanisms of ADIPOR1 mutants leading to hypertrophy and insulin resistance, or hypertrophy alone, respectively, events that ultimately cause cardiomyopathy.

that *ADIPOR1* mutations cause cardiac hypertrophy and fibrosis through the p38/mTOR and/or ERK pathways independent of AMPK. Notably, distended myocytes with vacuolated cytoplasm were absent in the ADIPOR1 mice (fig. S8, C and D). These findings suggest that *ADIPOR1*-associated HCM is functionally distinct from AMPK-associated glycogen storage cardiomyopathy.

We demonstrate that the overexpression of *ADIPOR1* mutations constitutively stimulates cardiac hypertrophy in cultured cardiomyocytes by increasing cell size, reactivating the fetal gene program, elevating leucine uptake, and activating the p38/mTOR and/or ERK1/2 pathways. *ADIPOR1* V146M transgenic mice recapitulate these cellular findings, displaying robust hypertrophy and fibrosis with chamber dilatation through mechanisms involving p38/mTOR activation. These mechanistic data support that p38/mTOR signaling pathways underlie a regulatory mechanism involved in the stimulation of cardiac hypertrophy and subsequently heart failure. Notably, p38 is an important regulator of fibrosis in cardiomyopathy (*25*), and interstitial fibrosis with collagen deposition has been shown to be strongly associated with LV hypertrophy in diabetic patients (*3*).

In contrast, F145I mutant activates the ERK1/2 pathway to cause hypertrophy that was rescued with the respective ERK1/2 inhibitor. The exact mechanisms and interplay between p38/mTOR and ERK1/2 signaling in cardiac dysfunction due to different *ADIPOR1* mutations remain to be elucidated. However, several previous lines of evidence suggest that these signaling cascades (the p38/mTOR and ERK pathways) can individually cause cardiac hypertrophy and fibrosis (*25*–*31*). In addition, treatment with APN (a well-known ADIPOR1 ligand) failed to inhibit the *ADIPOR1* mutant–induced activation of mTOR. These observations indicate that *ADIPOR1* mutants are sufficient to induce cardiac hypertrophy independent of ligand stimulation, further suggesting the loss of the beneficial cardioprotective effects of APN (*7*).

Cardiometabolic dysregulation in mutant ADIPOR1-induced HCM

Crucial mechanisms that lead to impairment in heart structure and function in individuals with diabetes are related to insulin sensitivity and glucose and lipid dysmetabolism. It is well established that APN and *ADIPOR1* play a central role in these processes and specifically in diabetes-associated cellular metabolism and mitochondrial function (*6*, *32*). In addition, *ADIPOR1* is known to play a prominent role in mediating the insulin-sensitizing effects of APN. The genetic ablation of *ADIPOR1*, *ADIPOR2*, or both in mouse models induces glucose intolerance and insulin resistance (*32*, *33*). Meanwhile, the deletion of *ADIPOR1* results in decreased AMPK activity and *Ppargc1a* expression and the induction of mitochondrial dysfunction (*32*). In line with these findings, we showed here that the V146M variant of *ADIPOR1* disrupted normal glucose transport and lipid metabolism and induced myocardial insulin resistance in vitro and in vivo. The V146M variant of *ADIPOR1* blunted the APN-induced stimulation of glucose uptake and significantly down-regulated the expression of key enzymes that regulate glucose utilization in cultured cardiomyocytes. In addition, the V146M variant of *ADIPOR1* inhibited insulin-stimulated glucose transport system in transgenic mouse

hearts. The impairment of the glycolytic pathways was further associated with a defect in insulin signaling, as demonstrated by the inhibition of insulin-stimulated AKT activity in cardiomyocytes and increased phosphorylation of IRS1 at serine residues 636/639 (*34*). Thus, our results suggest that the V146M *ADIPOR1* mutant modifies or contributes to the pathogenesis of cardiomyopathy by interfering with glucose uptake, blocking AKT activity, hyperphosphorylating IRS1, and down-regulating *Slc2a4*.

Insulin-stimulated glucose uptake is also affected by the accumulation of fatty acids through the inhibition of IRS and AKT activities. Our data demonstrated increased fatty acid utilization induced by the V146M variant of *ADIPOR1*. This may have been due to enhanced β-oxidation promoted by CPT-1 and the activation of PPARα/PGC-1α signaling. PPARα/PGC-1α control the transcription of key genes involved in fatty acid β-oxidation (such as *Slc2a4*, *Acox1*, and *Cpt1a*) and regulate energy balance and fatty acid utilization (*35*, *36*). Therefore, it is possible that the ADIPOR1 V146M–enhanced activation of PPARα signaling stimulates fatty acid oxidation, decreases the expression of insulin-responsive *Slc2a4*, and suppresses glucose oxidation and myocardial insulin responsiveness, possibly through feedback inhibition of glycolysis, including PFKM. The inhibition of p38 mitogen-activated protein kinase (MAPK) in our study normalized the V146M-induced fatty acid oxidation by reducing the expression of *Ppara* and *Cpt1a*, indicating that increased fatty acid oxidation occurs through a p38-dependent mechanism. Notably, all these features are induced by the V146M variant of *ADIPOR1* phenocopies to a greater extent of diabetic cardiomyopathic hearts (*37*, *38*). This is of particular interest, as most of the patients harboring the *ADIPOR1* variants have diabetes. Together, our findings suggest that myocardial insulin resistance induced by the expression of the V146M variant of *ADIPOR1* is potentially mediated by both excess fatty acid oxidation and p38/mTOR hyperactivation.

Rapamycin rescues the *ADIPOR1*-induced cardiomyopathy in mice

We have shown that the pharmacological inhibition of mTOR by rapamycin attenuates the hypertrophic response and metabolic dysregulation in both cellular and mouse models of *ADIPOR1* mutations. In *ADIPOR1* mice, the reversal of LV remodeling evoked by rapamycin was paralleled by a decrease in myocardial fibrosis, both interstitial and perivascular, improvements in cardiac performance and the enhancement of the SERCA2a/PLN ratio, leading to increased sarcoplasmic reticulum Ca^{2+} cycling and improved contractility. These findings provide support that the pharmacological inhibition of mTOR enhances cardiac function in V146M transgenic mice, potentially through a mechanism involving the up-regulation of SERCA2a activity and reduced cardiac fibrosis and hypertrophy. These data suggest that the activation of the mTOR pathway is critical for the *ADIPOR1*-induced hypertrophic response observed in patients with diabetes-associated HCM. mTOR is known to be an important positive regulator of protein synthesis and cell growth, which are key features of hypertrophy, and aberrant mTOR signaling has been implicated in an increasing number of pathological conditions, including cardiovascular disease and metabolic disorders (*28*, *29*, *31*), making this pathway a principle target for drug development. Notably, increased mTOR signaling is observed in various HCM mouse models caused by sarcomeric (*39*), RAS-MAPK signaling (*40*, *41*) and cytoskeletal mutations (*42*). In these models, the inhibition of mTOR by rapamycin was shown to ameliorate cardiomyopathy phenotypes, including fibrosis, and restore normal cardiac functions (*39*–*42*).

The present study is the first to identify clinically relevant pathological variants of the human *ADIPOR1* gene that primarily contribute to diabetes-associated HCM. Together, our results propose a mechanistic scenario in which in healthy individuals, *ADIPOR1* activates the AMPK pathway to provide cardioprotection, while mutant *ADIPOR1* activates the p38/mTOR and ERK pathways, inducing hypertrophy and metabolic defects and ultimately leading to cardiomyopathy (Fig. 6H). In conclusion, our data support *ADIPOR1* variants as novel contributors to HCM through excessive p38/mTOR and/or ERK activity and suggest that small chemical molecules that target these pathways might be beneficial for specific *ADIPOR1* mutated individuals (fig. S9).

MATERIALS AND METHODS

Clinical evaluations

A total of 2552 hospitalized, unrelated study patients along with 1894 controls with written informed consent were selected and obtained through various hospitals including Sri Jayadeva Institute of Cardiovascular Sciences and Research, Bengaluru, India. In addition, a total of 98 registered unrelated patients and their family members were obtained as we previously described (*5*, *41*). The institutional review boards of the study centers approved the study protocols.

Diagnostic criteria for the index individuals and controls

A standard international protocol was followed in diagnosing the cases, as we described previously (*5*), and the details of the baseline characteristics of the patients are given in table S1 (A and D). Briefly, individuals were diagnosed with HCM based on the following conventional criteria proposed by American Society of Echocardiography:

1) LV hypertrophy of ≥15 mm on two-dimensional echocardiography in the absence of another disease that could account for the hypertrophy.

2) LV septal to posterior wall thickness ratio of more than 1.3 in the absence of hypertension that could account for hypertrophy.

3) Nonobstructive HCM was defined as a pressure gradient of ≤30 mmHg at rest and after provocation. Patients with a pressure gradient of >30 mmHg at rest or after provocation were classified as obstructive HCM.

4) Any electrocardiogram (ECG) abnormalities along with the above echo-positive individuals: LV hypertrophy (Romhilt-Estes score, ≥4), Q-waves (a duration of >0.04 s and/or a depth of >1/4 of ensuring R wave in at least two leads), and marked repolarization abnormalities (T-wave inversion in at least two leads). Nonsustained ventricular tachycardia was defined as three or more ventricular extra systoles at a rate of ≥120 beats/min, lasting less than 30 s.

5) Family history was considered positive if anyone first degree relative had a clinical diagnosis of HCM.

6) For selective patients, cardiac magnetic resonance imaging was performed with the standard protocols including Cine, steady-state free precession (SSFP), T1-weighted, and T2-weighted imaging, followed by gadolinium administration and postgadolinium for late gadolinium enhancement (LGE) sequences using 1.5-T clinical system (Ingenia, Philips Healthcare, Best, The Netherlands). For LGE imaging, the

patient were administered with an intravenous injection of 0.2 mmol/kg of body weight gadolinium-based contrast reagent at 1 to 2 ml/s. Ten minutes after injection time, LGE images were acquired in the continuous short-axis view using an inversion-recovery gradient-recalled echo sequence using a manually selected optimal inversion time to null the signal from normal myocardium.

Two independent cardiologists verified the clinical diagnosis of the study individuals. Briefly, the patients' average septal thickness at the time of enrollment was 16 ± 4 cm, respectively. Diabetes was diagnosed if the glycosylated hemoglobin (HbA1c) levels were more than 6.5%, the fasting blood sugar level was ≥126 mg/dl, the 2-hour post-glucose value was ≥200 mg/dl, or it is a registered patient on drug therapy for diabetes. Further clinical details of the patients are outlined in table S1 (A and D).

The control group (n = 1894) was from the same geographic region similar to patients. The controls sex and age during the time of enrollment were as follows: 60% male and 40.02 ± 28 years, respectively. Population stratification analysis was performed using 50 ancestry-informative markers as described (*5*). The controls were apparently healthy volunteers with no family history or symptoms of cardiovascular diseases with a standard ECG and echocardiography parameters from the hospitals and were unrelated to the individuals with cardiomyopathy (*5*, *41*).

Assessment of family members

The unrelated index individuals (who are negative for sarcomeric disease mutations) and their parents participated in the present genetic study. The family members were assessed by ECG and echocardiography for their cardiac health status. Further clinical details of the patients are given in table S1D. The patient's family members who are clinically healthy are used as respective internal controls for identifying potential disease-causing mutations.

Whole-exome sequencing and analysis

Genomic DNA from the respective study individuals was isolated from peripheral blood lymphocytes using standard protocols (*5*). The DNA libraries were prepared and mixed with capture probes of targeted regions using protocols described by SureSelect V5 Target Enrichment kit (Agilent Genomics) (*43*). The enriched libraries were then amplified by polymerase chain reaction (PCR). Sequencing and targeted resequencing was performed using the respective service providers including institutional sequencing facility after deidentifying the patient details. The detail statistics including average read depth of the filtered variants, SNPs, and indels in the patients and their family members are outlined in table S1 (B and C). Briefly, for each exome, paired-end 100–base pair reads (100× coverage) was used, and 6-gigabyte data were obtained. The average coverage of the target region of the capture kit was 88, with 85% over 30× and 98% over 10×. Low-quality reads were filtered, and adapters were removed using Trimmomatic. Exome analysis and variant calling were performed using in-house custom pipeline. Exomes were first mapped on to the human reference genome (GRCh38) using Burrows-Wheeler aligner version 0.7 (BWA-MEM). Variant calling was performed using HaplotypeCaller from Genome Analysis Tool Kit (GATKv.3.4) (software.broadinstitute.org/gatk/). Variants were annotated using web interface of ANNOVAR software (wannovar.wglab.org/). The following parameters are considered as primary for prioritizing the variants: (i) coding regions; (ii) novel missense; (iii) ultrarare variants present less than 0.01% frequency (minor allele frequency, ≤0.01%) in the reference populations including dbSNP (version 142), 1000 Genomes Project, ESP, KOVA, Geno$_2$MP v2.2, TOPMed, ExAC, and gnomAD cohort alleles, Genome Asia 100K, healthy aging Indian exomes (www.idhans.org), and South Asian (Indian) healthy controls. The amino acid conservation across species was analyzed by comparing the protein sequences of various vertebrate species using the ClustalW2 software. (iv) Deleterious variants affecting potential protein functions were based on protein damage prediction softwares using Polymorphism Phenotyping v2 (PolyPhen2) (http://genetics.bwh.harvard.edu/pph2/), Sorting Intolerant From Tolerant (https://sift.bii.a-star.edu.sg/www/SIFT_dbSNP.html), and PANTHER-PSEP methods. Further, cardiovascular-related genes were filtered out using International Mouse Phenotyping Consortium (www.mousephenotype.org/) and Mouse Genome Informatics (www.informatics.jax.org/) databases. Last, a comprehensive literature survey was performed for understand the role of the particular genes in HCM and diabetes. To replicate the association of identified new gene variant, we performed targeted resequencing in various cohorts as outlined in table S1A.

For resequencing and confirmation, the exons and their flanking intronic boundaries of *ADIPOR1* were amplified from genomic DNA. Amplified PCR products were gel-isolated with a QIAEX II gel extraction kit (QIAGEN), sequenced on an ABI3730 DNA analyzer (PerkinElmer Corp., Applied Biosystems, Hitachi, Japan), using the BigDye Terminator Kit (Applied Biosystems), and analyzed on an ABI3730 DNA analyzer. Analysis of the likelihood of pathogenic effect of *ADIPOR1* mutation was carried out using the above outlined protein damage prediction tools (Fig. 1C). The amino acid conservation across species was analyzed by comparing the protein sequences of various vertebrate species using the ClustalW2 software.

Adenoviruses, cardiomyocytes preparation, and cell surface measurements

The *ADIPOR1* (AR1) mutations were introduced into a construct containing human *ADIPOR1* by site-directed mutagenesis (QuikChange Site-Directed Mutagenesis Kit, Stratagene). Recombinant adenoviruses encoding full-length human wild-type AR1 (Ad.AR1), mutants including Ad.V146M, Ad.L157H, and Ad.F145I along with the β-galactosidase (Ad.βGal) or green fluorescent protein (Ad.GFP) were prepared using the AdEasy Adenoviral Vector System (Stratagene, USA) and Invitrogen. Cardiomyocytes including neonatal, H9c2, and adult rat ventricular myocytes were isolated using standard techniques. As necessary, these cardiomyocytes were used for various experiments. Cells were divided into three groups; Ad.βGal-infected, Ad.AR1-infected, or AR1 mutant–infected cells (at a multiplicity of infection of 100). Four hours after infection, the media were replaced, and the cells were further incubated for 48 hours for neonatal or 24 hours for rat adult cardiomyocytes. In few experiments depending on the necessity, 10 or 15 min before harvesting, APN (30 μg/ml) or 100 nM insulin was added, respectively, as indicated. Cell surface areas were determined with ImageJ analyzer.

Immunocytochemical staining and fluorescence microscopy

For immunofluorescence studies, cardiomyocytes cultured on coverslips were washed with 1× phosphate-buffered saline (PBS) (Gibco, catalog no. 10010049) twice, 5 min each on mild shaking. Cells were fixed in 4% paraformaldehyde (Sigma-Aldrich, catalog

no. 158127) for 20 min at room temperature, again washed with 1× PBS, and permeabilized with 0.1% Triton X-100 (Sigma-Aldrich, catalog no. T8787) in PBS for 15 min at room temperature. Blocking was performed using 1% bovine serum albumin (HiMedia, catalog no. MB083) and 1% normal goat serum in PBS for 1 hour at room temperature. Cells were incubated with antibody against cardiac troponin T (catalog no. 5593S) overnight at 4°C. After washing cells with 1× PBS, three times, and cells were incubated with secondary antibody (Alexa Fluor 555, catalog no. A21428) for 1 hour at room temperature. After washing three times, cells were incubated with of phalloidin (Thermo Fisher Scientific, catalog no. A12379) as per the manufacturer's protocol for 1 hour at room temperature. Nuclear staining was performed using Hoechst dye (Thermo Fisher Scientific, catalog no. 62249). After washing cells twice, coverslips were mounted using VECTASHIELD antifade mounting medium (catalog no. H-1000). Images were collected using Olympus IX73 inverted fluorescence microscope system and then analyzed using ImageJ (Fiji) software.

Radioactivity assay

Glucose transport and fatty acid uptake assays were performed using 2-[1,2-3H(N)]-deoxy-D-glucose and [9,10-3H(N)]-palmitic acid, respectively. Isotopes were purchased from PerkinElmer. Radioactivity was counted by liquid scintillation spectroscopy (MicroBeta TriLux) and normalized to total protein content measured by bicinchoninic acid (BCA) protein assay kit (Pierce).

Real-time quantitative PCR analysis

Total RNA was isolated with TRIzol (Invitrogen) and synthesized to complementary DNA (cDNA) with qScript cDNA SuperMix (Quanta Biosciences). cDNA amount was quantified by real-time PCR with PerfeCta SYBR Green FastMix (Quanta Biosciences) using 7500 real-time PCR system (Applied Biosystems). The primers used are as follows: *Anf*, 5'-ACC TGC TAG ACC ACC TGG AGG AG-3′ and 5'-CCT TGG CTG TTA TCT TCG GTA CCG-3′; *Bnp*, 5'-GCT GCT TTG GGC ACA AGA TAG-3′ and 5′-GGT CTT CCT ACA ACA ACT TCA-3′; *Myh6*, 5′-GAG ATT TCT CCA ACC CAG-3′ and 5′- TCT GAC TTT CGG AGG TAC T-3′; *Myh7*, 5′-TTG GCA CGG ACT GCG TCA TC-3′ and 5′-GAG CCT CCA GAG TTT GCT GAA GGA-3′; *Slc27a1*, 5'-CCA TTGGTG ATG AAA AAG CA-3′ and 5′-GAT CGG CTT TAC CAA AGA TGT AG-3′; *Acox1*, 5′-TGT TAA GAA GAG TGC CAC CAT-3′ and 5'-ATC CAT CTC TTC ATA ACC AAA TTT-3′; *Cpt1a*-1, 5'-ACT CCT GGA AGA AGA AGT TCA-3′ and 5′-AGT ATC TTT GAC AGC TGG GAC-3′; *Ppargc1a*, 5′-ATA GAG TGT GCT GCC CTG GTT GGT-3′ and 5′-TGG TCA CTA CAC CAC TTCAAT CCA-3′; *Ppara*, 5'-ACT ACG GAG TTC ACG CAT GTG-3′ and 5′-TTG TCG TAC ACC AGC TTC AGC-3′; *Slc2a1*, 5'-CAG TTC GGC TAT AAC ACT GGT G-3′ and 5′- GCC CCC GAC AGA GAA GAT G; *Slc2a4*, 5'-GAC GGA CAC TCC ATC TGT TG-3′ and 5'-CAT AGC TCATGG CTG GAA CC; *Pfkm*, 5'-CAG ATC AGT GCC AAC ATA ACC AA-3′ and 5'-CGG GAT GCA GAG CTC ATC A-3′; *18S rRNA*, 5'-TCA AGA ACG AAA GTC GGA GG-3′ and 5′-GGA CAT CTA AGG GCA TCA C-3′. Fold changes in gene expression were determined using the relative comparison method with normalization to 18*S* ribosomal RNA (rRNA).

Immunoblotting analysis

Cultured cardiomyocytes and total heart tissue were homogenized in radioimmunoprecipitation assay buffer containing protease (Roche) and phosphatase (Sigma-Aldrich) inhibitors. Thirty micrograms of protein were applied to SDS–polyacrylamide gel electrophoresis and transferred onto nitrocellulose membrane. The following antibodies obtained from Cell Signaling Technology were used: phospho- or total AMPKα, LKB1, ACC, AKT, ERK, p38, mTOR, $p70^{S6K}$, eEF2K, eEF2, IRS1, PFK2, Serca2a, PLN, ADIPOR1, COX2, β-actin, and glyceraldehyde-3-phosphate dehydrogenase (GAPDH). The membranes were incubated with appropriate secondary antibodies, and signal intensities were visualized with enhanced chemiluminescence (Pierce). Total protein contents of the corresponding proteins were analyzed after stripping the phospho-blots to verify protein loading. GAPDH or β-actin was used as internal loading controls. To study the inhibition effects of p38, ERK1/2, and mTOR on cardiac hypertrophy and signaling pathways, cells were treated with corresponding pharmacological inhibitors (10 μM SB203580 for p38 and 100 nM rapamycin for mTOR for 30 min before harvesting or PD325901 for ERK1/2).

Generation of conditional ADIPOR1 Cre-V146M transgenic mice

Cardiac-specific expression of a representative *ADIPOR1* variant (Cre-V146M) was achieved using a standard "gene switch" strategy. Briefly, the human ADIPOR1 mutant (GFP-tagged AR1-V146M) was inserted into the pMHC-flox vector (a gift from Y. Wang) to generate the pMHC-flox-AR1V146M construct. The construct was microinjected into fertilized eggs from B6C3 mice, and transgenic integration was confirmed by PCR. Heterozygote AR1V146M-flox/+ mice were crossed with heterozygote αMHC-Mer-Cre-Mer mice (MCM±; the Jackson laboratory). Cre-mediated overexpression of AR1-V146M was induced by oral delivery of tamoxifen (Sigma-Aldrich) for five consecutive days of the same dose (30 μg/g reconstituted in peanut oil). Using this system, we established two transgenic lines (fig. S7A). The transgene copy numbers/expression was quantified using GFP in Cre-V146M compared to Cre mice (fig. S7B). Both the mouse lines were viable and had a healthy and average life span, generally suggesting an unlikely event of any overtly off-targets phenotypes. All analyses were performed on mixed heterozygote AR1-V146M-flox/+/MCM± transgenic mice (Cre-V146M) and sex-matched littermates (Cre).

Ultrasound imaging and analyses

Animals were handled as approved by the respective Institutional Animal Care and Use Committees in accordance with the "Principles of Laboratory Animal Care by the National Society for Medical research and the Guide for the Care and Use of Laboratory Animals" (NIH Publication No. 86-23, revised 1996).

Echocardiography

Transgenic (Cre-V146M) and control (Cre) mice (12 to 13 weeks of age) were anesthetized after 8 weeks after tamoxifen treatment with intraperitoneal ketamine (100 mg/kg) for echocardiographic analysis. Two-dimensional images and M-mode tracings were recorded on the short axis at the level of the papillary muscle to determine the percentage FS and ventricular dimensions (GE Vivid 7 Vision) as we previously described (*44*).

Rapamycin studies

Cre-V146M and Cre mice at 12 weeks of age were treated with rapamycin (2 mg/kg; LC Laboratories) (intraperitoneally, dissolved in 4% ethanol, 0.25% PEG300, and 0.25% Tween 80) or vehicle every other day for 30 days. Rapamycin injections were started at 8 weeks after tamoxifen stimulation.

Histological analyses

Histological assessment of fibrosis

To assess cardiac fibrosis, serial 8-μm frozen sections from LV tissue were stained with standard Masson trichrome following the manufacturer's instructions (Sigma-Aldrich).

Cross-sectional area measurements

Cardiomyocyte cross-sectional area was determined with fluorescein-conjugated or Texas Red–conjugated wheat-germ agglutinin (5 μg/ml; Invitrogen). The areas of approximately 100 myocytes with circular shape of the cell membrane were measured in the LV free walls of each animal, using ImageJ software. Myocardial fibrosis staining images were acquired at 20× magnification under circular polarized illumination using an Olympus BX50 microscope (Olympus, Melville, NY). The relative amount of collagen area to total tissue area was measured in each image using a color threshold technique using the ImageJ software.

Insulin treatment

Mice were fasted overnight and received a single intraperitoneal injection of body weight insulin (10 mU/g) 10 min before the hearts were harvested (*45*).

Statistical analysis

The summary statistics for whole exome including average read depth of the filtered variants, SNPs, and indels in the patients and their family members are outlined in table S1 (B and C). For other experiments, statistical significance analysis was determined by two-tailed Student's *t* test and one-way or two-way analysis of variance (ANOVA) with appropriate post hoc analysis. $P < 0.05$ was considered to be statistically significant.

SUPPLEMENTARY MATERIALS

Supplementary material for this article is available at http://advances.sciencemag.org/cgi/content/full/7/2/eabb3991/DC1

View/request a protocol for this paper from *Bio-protocol*.

REFERENCES AND NOTES

1. E. M. Mcnally, D. Y. Barefield, M. J. Puckelwartz, The genetic landscape of cardiomyopathy and its role in heart failure. *Cell Metab.* **21**, 174–182 (2015).
2. N. Frey, M. Luedde, H. A. Katus, Mechanisms of disease: Hypertrophic cardiomyopathy. *Nat. Rev. Cardiol.* **9**, 91–100 (2011).
3. Y. Wasserstrum, R. Barriales-Villa, X. Fernández-Fernández, Y. Adler, D. Lotan, Y. Peled, R. Klempfner, R. Kuperstein, N. Shlomo, A. Sabbag, D. Freimark, L. Monserrat, M. Arad, The impact of diabetes mellitus on the clinical phenotype of hypertrophic cardiomyopathy. *Eur. Heart J.* **40**, 1671–1677 (2019).
4. M. A. Burke, S. A. Cook, J. G. Seidman, C. E. Seidman, Clinical and mechanistic insights into the genetics of cardiomyopathy. *J. Am. Coll. Cardiol.* **68**, 2871–2886 (2016).
5. P. S. Dhandapany, S. Sadayappan, Y. Xue, G. T. Powell, D. S. Rani, P. Nallari, T. S. Rai, M. Khullar, P. Soares, A. Bahl, J. M. Tharkan, P. Vaideeswar, A. Rathinavel, C. Narasimhan, D. R. Ayapati, Q. Ayub, S. Q. Mehdi, S. Oppenheimer, M. B. Richards, A. L. Price, N. Patterson, D. Reich, L. Singh, C. Tyler-Smith, K. Thangaraj, A common *MYBPC3* (cardiac myosin binding protein C) variant associated with cardiomyopathies in South Asia. *Nat. Genet.* **41**, 187–191 (2009).
6. M. Iwabu, T. Yamauchi, M. Okada-Iwabu, K. Sato, T. Nakagawa, M. Funata, M. Yamaguchi, S. Namiki, R. Nakayama, M. Tabata, H. Ogata, N. Kubota, I. Takamoto, Y. K. Hayashi, N. Yamauchi, H. Waki, M. Fukayama, I. Nishino, K. Tokuyama, K. Ueki, Y. Oike, S. Ishii, K. Hirose, T. Shimizu, K. Touhara, T. Kadowaki, Adiponectin and AdipoR1 regulate PGC-1α and mitochondria by Ca^{2+} and AMPK/SIRT1. *Nature* **464**, 1313–1319 (2010).
7. N. Ouchi, R. Shibata, K. Walsh, Cardioprotection by adiponectin. *Trends Cardiovasc. Med.* **16**, 141–146 (2006).
8. R. Shibata, K. Sato, D. R. Pimentel, Y. Takemura, S. Kihara, K. Ohashi, T. Funahashi, N. Ouchi, K. Walsh, Adiponectin protects against myocardial ischemia-reperfusion injury through AMPK- and COX-2–dependent mechanisms. *Nat. Med.* **11**, 1096–1103 (2005).
9. R. Shibata, N. Ouchi, M. Ito, S. Kihara, I. Shiojima, D. R. Pimentel, M. Kumada, K. Sato, S. Schiekofer, K. Ohashi, T. Funahashi, W. S. Colucci, K. Walsh, Adiponectin-mediated modulation of hypertrophic signals in the heart. *Nat. Med.* **10**, 1384–1389 (2004).
10. D. Fujioka, K.-i. Kawabata, Y. Saito, T. Kobayashi, T. Nakamura, Y. Kodama, H. Takano, J.-e. Obata, Y. Kitta, K. Umetani, K. Kugiyama, Role of adiponectin receptors in endothelin-induced cellular hypertrophy in cultured cardiomyocytes and their expression in infarcted heart. *Am. J. Physiol. Heart Circ. Physiol.* **290**, H2409–H2416 (2006).
11. H. Kondo, I. Shimomura, Y. Matsukawa, M. Kumada, M. Takahashi, M. Matsuda, N. Ouchi, S. Kihara, T. Kawamoto, S. Sumitsuji, T. Funahashi, Y. Matsuzawa, Association of adiponectin mutation with type 2 diabetes: A candidate gene for the insulin resistance syndrome. *Diabetes* **51**, 2325–2328 (2002).
12. K. Ohashi, N. Ouchi, S. Kihara, T. Funahashi, T. Nakamura, S. Sumitsuji, T. Kawamoto, S. Matsumoto, H. Nagaretani, M. Kumada, Y. Okamoto, H. Nishizawa, K. Kishida, N. Maeda, H. Hiraoka, Y. Iwashima, K. Ishikawa, M. Ohishi, T. Katsuya, H. Rakugi, T. Ogihara, Y. Matsuzawa, Adiponectin I164T mutation is associated with the metabolic syndrome and coronary artery disease. *J. Am. Coll. Cardiol.* **43**, 1195–1200 (2004).
13. R. Palanivel, X. Fang, M. Park, M. Eguchi, S. Pallan, S. De Girolamo, Y. Liu, Y. Wang, A. Xu, G. Sweeney, Globular and full-length forms of adiponectin mediate specific changes in glucose and fatty acid uptake and metabolism in cardiomyocytes. *Cardiovasc. Res.* **75**, 148–157 (2007).
14. T. Yamauchi, J. Kamon, Y. Minokoshi, Y. Ito, H. Waki, S. Uchida, S. Yamashita, M. Noda, S. Kita, K. Ueki, K. Eto, Y. Akanuma, P. Froguel, F. Foufelle, P. Ferre, D. Carling, S. Kimura, R. Nagai, B. Kahn, T. Kadowaki, Adiponectin stimulates glucose utilization and fatty-acid oxidation by activating AMP-activated protein kinase. *Nat. Med.* **8**, 1288–1295 (2002).
15. X. Mao, C. K. Kikani, R. A. Riojas, P. Langlais, L. Wang, F. J. Ramos, Q. Fang, C. Y. Christ-Roberts, J. Y. Hong, R.-Y. Kim, F. Liu, L. Q. Dong, APPL1 binds to adiponectin receptors and mediates adiponectin signalling and function. *Nat. Cell Biol.* **8**, 516–523 (2006).
16. B. N. Finck, The PPAR regulatory system in cardiac physiology and disease. *Cardiovasc. Res.* **73**, 269–277 (2007).
17. S. J. Buss, S. Muenz, J. H. Riffel, P. Malekar, M. Hagenmueller, C. S. Weiss, F. Bea, R. Bekeredjian, M. Schinke-Braun, S. Izumo, H. A. Katus, S. E. Hardt, Beneficial effects of mammalian target of rapamycin inhibition on left ventricular remodeling after myocardial infarction. *J. Am. Coll. Cardiol.* **54**, 2435–2446 (2009).
18. X.-M. Gao, G. Wong, B. Wang, H. Kiriazis, X.-L. Moore, Y.-D. Su, A. Dart, X.-J. Du, Inhibition of mTOR reduces chronic pressure-overload cardiac hypertrophy and fibrosis. *J. Hypertens.* **24**, 1663–1670 (2006).
19. M. Völkers, M. H. Konstandin, S. Doroudgar, H. Toko, P. Quijada, S. Din, A. Joyo, L. Ornelas, K. Samse, D. J. Thuerauf, N. Gude, C. C. Glembotski, M. A. Sussman, Mechanistic target of rapamycin complex 2 protects the heart from ischemic damage. *Circulation* **128**, 2132–2144 (2013).
20. R. N. Saunders, M. S. Metcalfe, M. L. Nicholson, Rapamycin in transplantation: A review of the evidence. *Kidney Int.* **59**, 3–16 (2001).
21. I.-P. Chou, Y.-P. Chiu, S.-T. Ding, B.-H. Liu, Y. Y. Lin, C.-Y. Chen, Adiponectin receptor 1 overexpression reduces lipid accumulation and hypertrophy in the heart of diet-induced obese mice–possible involvement of oxidative stress and autophagy. *Endocr. Res.* **39**, 173–179 (2014).
22. J. T. Hinson, A. Chopra, A. Lowe, C. C. Sheng, R. M. Gupta, R. Kuppusamy, J. O'Sullivan, G. Rowe, H. Wakimoto, J. Gorham, M. A. Burke, K. Zhang, K. Musunuru, R. E. Gerszten, S. M. Wu, C. S. Chen, J. G. Seidman, C. E. Seidman, Integrative analysis of PRKAG2 cardiomyopathy iPS and microtissue models identifies AMPK as a regulator of metabolism, survival, and fibrosis. *Cell Rep.* **17**, 3292–3304 (2016).
23. M. Kim, R. W. Hunter, L. Garcia-Menendez, G. Gong, Y.-Y. Yang, S. C. Kolwicz Jr., J. Xu, K. Sakamoto, W. Wang, R. Tian, Mutation in the γ2-subunit of AMP-activated protein kinase stimulates cardiomyocyte proliferation and hypertrophy independent of glycogen storage. *Circ. Res.* **114**, 966–975 (2014).
24. R. T. Murphy, J. Mogensen, K. Mcgarry, A. Bahl, A. Evans, E. Osman, P. Syrris, G. Gorman, M. Farrell, J. L. Holton, M. G. Hanna, S. Hughes, P. M. Elliott, C. A. MacRae, W. J. McKenna, Adenosine monophosphate-activated protein kinase disease mimicks hypertrophic cardiomyopathy and Wolff-Parkinson-White syndrome: Natural history. *J. Am. Coll. Cardiol.* **45**, 922–930 (2005).
25. T. Yokota, Y. Wang, p38 MAP kinases in the heart. *Gene* **575**, 369–376 (2016).
26. M. S. Marber, B. Rose, Y. Wang, The p38 mitogen-activated protein kinase pathway—A potential target for intervention in infarction, hypertrophy, and heart failure. *J. Mol. Cell. Cardiol.* **51**, 485–490 (2011).
27. I. Kehat, J. Davis, M. Tiburcy, F. Accornero, M. K. Saba-El-Leil, M. Maillet, A. J. York, J. N. Lorenz, W. H. Zimmermann, S. Meloche, J. D. Molkentin, Extracellular signal-regulated kinases 1 and 2 regulate the balance between eccentric and concentric cardiac growth. *Circ. Res.* **108**, 176–183 (2011).
28. S. Sciarretta, M. Volpe, J. Sadoshima, Mammalian target of rapamycin signaling in cardiac physiology and disease. *Circ. Res.* **114**, 549–564 (2014).
29. S. Sciarretta, M. Forte, G. Frati, J. Sadoshima, New insights into the role of mTOR signaling in the cardiovascular system. *Circ. Res.* **122**, 489–505 (2018).

30. M.-H. Lee, R. L. Klein, H. M. El-Shewy, D. K. Luttrell, L. M. Luttrell, The adiponectin receptors AdipoR1 and AdipoR2 activate ERK1/2 through a Src/Ras-dependent pathway and stimulate cell growth. *Biochemistry* **47**, 11682–11692 (2008).
31. E. Dazert, M. N. Hall, mTOR signaling in disease. *Curr. Opin. Cell Biol.* **23**, 744–755 (2011).
32. T. Yamauchi, Y. Nio, T. Maki, M. Kobayashi, T. Takazawa, M. Iwabu, M. Okada-Iwabu, S. Kawamoto, N. Kubota, T. Kubota, Y. Ito, J. Kamon, A. Tsuchida, K. Kumagai, H. Kozono, Y. Hada, H. Ogata, K. Tokuyama, M. Tsunoda, T. Ide, K. Murakami, M. Awazawa, I. Takamoto, P. Froguel, K. Hara, K. Tobe, R. Nagai, K. Ueki, T. Kadowaki, Targeted disruption of AdipoR1 and AdipoR2 causes abrogation of adiponectin binding and metabolic actions. *Nat. Med.* **13**, 332–339 (2007).
33. M. Bjursell, A. Ahnmark, M. Bohlooly-Y, L. William-Olsson, M. Rhedin, X.-R. Peng, K. Ploj, A.-K. Gerdin, G. Arnerup, A. Elmgren, A.-L. Berg, J. Oscarsson, D. Lindén, Opposing effects of adiponectin receptors 1 and 2 on energy metabolism. *Diabetes* **56**, 583–593 (2007).
34. Y. Qi, Z. Xu, Q. Zhu, C. Thomas, R. Kumar, H. Feng, D. E. Dostal, M. F. White, K. M. Baker, S. Guo, Myocardial loss of IRS1 and IRS2 causes heart failure and is controlled by p38α MAPK during insulin resistance. *Diabetes* **62**, 3887–3900 (2013).
35. B. N. Finck, D. P. Kelly, Peroxisome proliferator–activated receptor γ coactivator-1 (PGC-1) regulatory cascade in cardiac physiology and disease. *Circulation* **115**, 2540–2548 (2007).
36. R. Ventura-Clapier, A. Garnier, V. Veksler, Transcriptional control of mitochondrial biogenesis: The central role of PGC-1α. *Cardiovasc. Res.* **79**, 208–217 (2008).
37. D. An, B. Rodrigues, Role of changes in cardiac metabolism in development of diabetic cardiomyopathy. *Am. J. Physiol. Heart Circ. Physiol.* **291**, H1489–H1506 (2006).
38. P. J. Randle, P. B. Garland, C. N. Hales, E. A. Newsholme, The glucose fatty-acid cycle its role in insulin sensitivity and the metabolic disturbances of diabetes mellitus. *Lancet* **281**, 785–789 (1963).
39. S. R. Singh, A. T. L. Zech, B. Geertz, S. Reischmann-Düsener, H. Osinska, M. Prondzynski, E. Krämer, Q. Meng, C. Redwood, J. van der Velden, J. Robbins, S. Schlossarek, L. Carrier, Activation of autophagy ameliorates cardiomyopathy in *Mybpc3*-targeted knockin mice. *Circ. Heart Fail.* **10**, e004140 (2017).
40. T. M. Marin, K. Keith, B. Davies, D. A. Conner, P. Guha, D. Kalaitzidis, X. Wu, J. Lauriol, B. Wang, M. Bauer, R. Bronson, K. G. Franchini, B. G. Neel, M. I. Kontaridis, Rapamycin reverses hypertrophic cardiomyopathy in a mouse model of LEOPARD syndrome–associated *PTPN11* mutation. *J. Clin. Investig.* **121**, 1026–1043 (2011).
41. P. S. Dhandapany, M. A. Razzaque, U. Muthusami, S. Kunnoth, J. J. Edwards, S. Mulero-Navarro, I. Riess, S. Pardo, J. Sheng, D. S. Rani, B. Rani, P. Govindaraj, E. Flex, T. Yokota, M. Furutani, T. Nishizawa, T. Nakanishi, J. Robbins, G. Limongelli, R. J. Hajjar, D. Lebeche, A. Bahl, M. Khullar, A. Rathinavel, K. C. Sadler, M. Tartaglia, R. Matsuoka, K. Thangaraj, B. D. Gelb, *RAF1* mutations in childhood-onset dilated cardiomyopathy. *Nat. Genet.* **46**, 635–639 (2014).
42. J. C. Choi, A. Muchir, W. Wu, S. Iwata, S. Homma, J. P. Morrow, H. J. Worman, Temsirolimus activates autophagy and ameliorates cardiomyopathy caused by lamin A/C gene mutation. *Sci. Transl. Med.* **4**, 144ra102 (2012).
43. J. Xu, Z. Li, X. Ren, M. Dong, J. Li, X. Shi, Y. Zhang, W. Xie, Z. Sun, X. Liu, Q. Dai, Investigation of pathogenic genes in Chinese sporadic hypertrophic cardiomyopathy patients by whole exome sequencing. *Sci. Rep.* **5**, 16609 (2015).
44. N. Hammoudi, D. Jeong, R. Singh, A. Farhat, M. Komajda, E. Mayoux, R. Hajjar, D. Lebeche, Empagliflozin improves left ventricular diastolic dysfunction in a genetic model of type 2 diabetes. *Cardiovasc. Drugs Ther.* **31**, 233–246 (2017).
45. D. D. Belke, S. Betuing, M. J. Tuttle, C. Graveleau, M. E. Young, M. Pham, D. Zhang, R. C. Cooksey, D. A. Mcclain, S. E. Litwin, H. Taegtmeyer, D. Severson, C. R. Kahn, E. D. Abel, Insulin signaling coordinately regulates cardiac size, metabolism, and contractile protein isoform expression. *J. Clin. Invest.* **109**, 629–639 (2002).

Acknowledgments: We thank all participants for making this study possible. We acknowledge the technical help of Perundurai laboratory members including K. Bose and A. Mittal. **Funding:** P.S.D. is supported by the Wellcome Trust Indian Alliance, Rajiv Gandhi University of Health Sciences (RGUHS), Scientist Development Grant (SDG) from American Heart Association (AHA), and inStem core funding. K.T. was supported by the JC Bose Fellowship from SERB, DST, and government of India. N.R.S. is supported by funding from Advanced Research Department, RGUHS, and Indian Institute of Science, Department of Biotechnology partnership program for advanced research. S.K. was supported by a postdoctoral fellowship from the AHA. D.L. is supported by grants from the NIH. **Author contributions:** P.S.D. and D.L. designed the study, analyzed the data, and wrote the manuscript. P.S.D. is involved in patient novel gene discovery and related functional characterization for HCM. P.S.D., S.K., D.K.K., and D.L. were involved in functional genomics studies. P.S.D., D.L., R.R., N.R.S., R.S., and K.T. provided reagents for the study. S.J., C.N.M., and J.S. helped in clinical evaluation of the patients. **Competing interests:** The authors declare that they have no competing interests. **Data and materials availability:** All data needed to evaluate the conclusions in the paper are present in the paper and/or the Supplementary Materials. Additional data related to this paper may be requested from the authors.

Submitted 21 February 2020
Accepted 13 November 2020
Published 6 January 2021
10.1126/sciadv.abb3991

Citation: P. S. Dhandapany, S. Kang, D. K. Kashyap, R. Rajagopal, N. R. Sundaresan, R. Singh, K. Thangaraj, S. Jayaprakash, C. N. Manjunath, J. Shenthar, D. Lebeche, Adiponectin receptor 1 variants contribute to hypertrophic cardiomyopathy that can be reversed by rapamycin. *Sci. Adv.* **7**, eabb3991 (2021).

Science Advances

Adiponectin receptor 1 variants contribute to hypertrophic cardiomyopathy that can be reversed by rapamycin

Perundurai S. Dhandapany, Soojeong Kang, Deepak K. Kashyap, Raksha Rajagopal, Nagalingam R. Sundaresan, Rajvir Singh, Kumarasamy Thangaraj, Shilpa Jayaprakash, Cholenahally N. Manjunath, Jayaprakash Shenthar and Djamel Lebeche

Sci Adv **7** (2), eabb3991.
DOI: 10.1126/sciadv.abb3991